

Barbora Bittová; J. Poltíerová-Vejpravová; S. Burianová; M. Kalbac; S. Danis
Seeking intrinsic magnetism in carbon nanotubes

Acta Universitatis Carolinae. Mathematica et Physica, Vol. 53 (2012), No. 1, 33--[42]

Persistent URL: <http://dml.cz/dmlcz/143687>

Terms of use:

© Univerzita Karlova v Praze, 2012

Institute of Mathematics of the Academy of Sciences of the Czech Republic provides access to digitized documents strictly for personal use. Each copy of any part of this document must contain these *Terms of use*.



This paper has been digitized, optimized for electronic delivery and stamped with digital signature within the project *DML-CZ: The Czech Digital Mathematics Library* <http://project.dml.cz>

SEEKING INTRINSIC MAGNETISM IN CARBON NANOTUBES

B. BITTOVÁ, J. POLTIEROVÁ-VEJPRTRAVOVÁ, S. BURIANOVÁ, M. KALBAC, S. DANIS

Praha

Received June 14, 2011

Revised September 15, 2011

We have investigated magnetic response of residual metal catalyst in the raw and super purified HiPco single wall carbon nanotubes (HiPco_raw and HiPco_SP SWCNTs). Also several techniques leading to removal of metal catalyst, such as oxidation in mild acid and high temperature annealing have been performed. It has been shown in case of commercial and commercially purified (HiPco_raw and SP) SWCNTs that the residual metal catalyst is in the form of nanoparticles even in the HiPco_SP SWCNTs that should contain minimal amount of the metal. Mössbauer spectroscopy of the HiPco_raw SWCNTs proved the catalyst nanoparticles are in the form of Fe_3C . Analysis of the synchrotron X-ray diffraction measurement together with magnetic studies by means of temperature dependence of magnetization, magnetization isotherms and susceptibility suggested a core-shell structure of the nanoparticles in the HiPco_raw SWCNTs, with a magnetically oriented core and a paramagnetic shell, which is almost removed in case of the HiPco_SP catalyst nanoparticles. Analysis of purified samples showed that in most cases, the residual metal also remains in form of sintered nanoparticles with reduced shell part. Only the high temperature annealed SWCNTs exhibited diamagnetic response, pointing at the high purity of SWCNTs, even much better than is the purity of commercially purified HiPco_SP SWCNTs.

Institute of Physics of the ASCR, v.v.i., Na Slovance 2, 182 21 Prague 8, Czech Republic (B. Bittová, J. Poltierová-Vejprtravová, S. Burianová)

J. Heyrovsky Institute of Physical Chemistry of the ASCR, v.v.i., Dolejskova 3, 18223 Prague 8, Czech Republic (M. Kalbac)

Charles University in Prague, Faculty of Mathematics and Physics, Department of Condensed Matter Physics, Ke Karlovu 5, 121 19 Prague 2, Czech Republic (S. Danis)

This work was supported by the Grant Agency of the Czech Republic under project no. P204/10/1677. We also thank to synchrotron radiation source ANKA in Karlsruhe for providing the beamtime.

Key words and phrases. Carbon nanotubes, intrinsic magnetism

E-mail address: bittova@fzu.cz

1. Introduction

Since the magnetism and superconductivity of the pure carbon materials has been theoretically predicted and already observed in special cases (magnetic ordering in the proton-irradiated graphite [Esquinazi *et al.*, 2003], pressure induced magnetism in fullerenes [Makarova *et al.*, 2001]), the possibility to study and utilize magnetic response of carbon nanotubes (CNTs) for further applications in spintronics has appeared recently.

The CNTs could possess not even the semiconducting and metallic properties, depending on their chirality, but it has been also proved theoretically that the metallic CNTs could exhibit ferromagnetic ground state [Dresselhaus *et al.*, 2001, Montioux *et al.*, 2001]. In spite of these studies discussing the defect—induced magnetism in CNTs, this phenomenon has not been experimentally observed yet. It is mainly because of presence of the residual metal catalyst in the nanotubes and its untrivial removal.

Because of mentioned reasons, purification of the CNTs started to be the crucial point. Many reports about the chemical and physical methods of purification have been published since the year 2006, but only the few ones gave the evidence of the removal of residual catalyst supported by the comprehensive experimental analysis.

Because of that, we have tried several approaches of purification of nanotubes and investigated the properties of purified nanotubes by methods that provided us the comprehensive information about the amount and nature of residual catalyst. Not only the proportional amount of the metal in the sample is important, but also the form in which this metal is presented, because the magnetic response is different whether there are the nanoparticles or the single atoms.

Because the magnetic properties of the catalyst in the non-purified commercially available nanotubes were not studied yet, we have started with the deep investigation of HiPco raw SWCNTs [Bittova *et al.*, 2011]. Also the HiPco_SP SWCNTs were studied to have the comparison of commercial and laboratory methods of purification. Discussion on magnetic properties of nanoparticles is based on the superparamagnetism and related phenomena considering interparticle interactions [Neel *et al.*, 1949].

2. Experimental section

At first, the commercially available HiPco_raw and HiPco_SP nanotubes were investigated. Then the several purification processes were performed on the HiPco_raw nanotubes, such as 1. low temperature annealing (400 °C) followed by the reflux in mixture of HCl and H₂O₂ (sample labelled as HiPco_400), 2. annealing at 1200 °C in static vacuum (HiPco_1200) and 3. high temperature vacuum annealing at 2200 °C (HiPco_2200).

The samples have been characterized by several methods to gain comprehensive amount of data to analyze properly properties of the metal catalyst.

Thermogravimetry (TG) has been used for setting the mass content of the metal precursor in the SWCNTs. The samples were heated up to the 800 °C with the heating rate of 10 K/min in atmosphere containing 80% of He and 20% of O₂.

We have used complementary methods for the phase analysis and particle size determination, respectively. The synchrotron radiation diffraction (S-XRD) was used for determination of catalyst phase and for estimation of the mean diameter of the catalyst particles in the HiPco_raw and HiPco_SP SWCNTs, respectively. The diffraction data has been taken at PDIFF beamline in ANKA Karlsruhe, using the radiation with wavelength of 1.24 Å. The diffraction patterns were collected within the range of 3–63 ° with the step of 0.02 °. Further analyses have been done using FullProf software [Willes and Young, 1982].

The Mössbauer spectra were employed as a complementary experiment to determine the iron phase in the HiPco_raw sample. The measurement was done in the transmission mode with ⁵⁷Co diffused into the Rh matrix as the source moving with constant acceleration. The spectrometer was calibrated by means of a standard Fe foil and the isomer shift was expressed with respect to this standard at 293 K. The HiPco_raw sample was measured in cryostat at the temperatures varying from 293 to 4.2 K. The fitting of the spectra was performed with the help of the NORMOS program. The samples seem not to be suitable for the experiment because of the undetectable amount of metal catalyst.

Magnetic measurements on all HiPco SWCNTs were performed using MPMS7 – SQUID device (Quantum Design) up to magnetic field of 7 T in the temperature range 2–400 K. The zero-field-cooled (ZFC) and field-cooled (FC) curves were measured in low external magnetic fields (from 5 to 50 mT). The magnetization isotherms were measured at 10 and 300 K up to field of 7 T in both polarities. The temperature dependence of the a.c. susceptibility (with the alternating field amplitude of 3 mT) was measured in non-zero magnetic field (1–100 mT) in frequency range of 0.1–100 Hz.

3. Results and discussion

3.1 Analysis of compound and structure

TG provided the mass content of metal precursor in the samples leading to the values of 75 wt% for the HiPco_raw, 5 wt% for the HiPco_SP, 25 wt% for the HiPco_1200 and 0 wt% for the HiPco_2200 SWCNTs (Figure 1). The mild acid treated sample (HiPco_400) was not analysed because the amount of the sample was not sufficient.

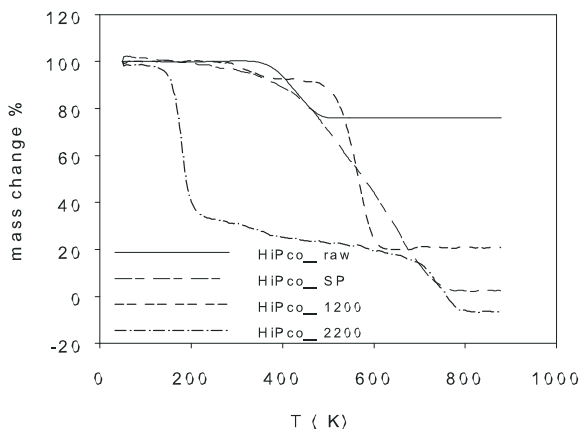


FIGURE 1. The thermogravimetry data of all samples.

The S-XRD pattern of the HiPco_raw SWCNTs reveals the peak positions corresponding to those of the cementite, Fe_3C (Figure 2), which crystallizes in the orthorhombic Pnma space group with the four units in the unit cell ($Z=4$) [Shein *et al.*, 2007]. The eight of the iron atoms are in 8d positions (Fe_g), four are placed in 4c positions (Fe_s) and the four carbon atoms sit in the interstitials. Because the quality of the diffraction pattern has not been suitable for the full profile fitting procedure by the Rietveld method, the mean size of the Fe_3C particles was calculated from the (102) and (201) reflections, leading to the value of 1.9 nm, considering the resolution function.

The PXRD pattern of the HiPco_400 and the HiPco_1200 samples provided presence both of Fe_3C and Fe_2O_3 phases, confirming the partial removal of carbonous shell encapsulating nanoparticles and subsequent oxidation of metal particles (data are not presented).

The Mössbauer spectroscopy confirmed the presence of Fe_3C -cementite phase in the HiPco_raw sample. No metal iron (zero isomer shift) has been detected. The room temperature spectrum consists of doublet indicating the superparamagnetic state of the sample that can be attributed to the small size of Fe_3C particles in nanotubes. The spectrum was fitted with two doublets representing the two types of sites for iron atoms—the general (Fe_g) and special (Fe_s) sites (Figure 2). The intensities of lines were fixed up to 2:1. The obtained parameters are in good agreement with those presented by other authors [Ron and Mathalone, 1971].

3.2 Magnetization studies and hysteresis

The zero-field-cooled (ZFC) and field-cooled (FC) curves (Figures 3–6) exhibit the main attributes of the superparamagnetic (SPM) systems. The ZFC curves exhibit sharp maximum at the temperature T_{MAX} representing blocking temperature T_B

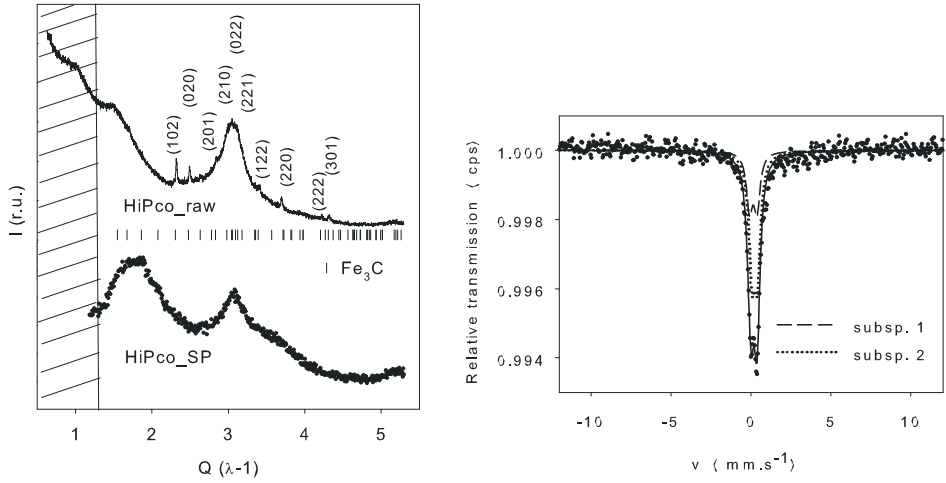


FIGURE 2. Left: S-XRD patterns for the HiPco_raw and HiPco_SP SWCNTs. The vertical marks correspond to the positions of the Fe_3C Bragg reflections, the cross—hatched area illustrates expected positions of the SWCNTs reflections. Right: Fit of the Mössbauer spectra measured at room temperature by the two subspectra, representing the two special positions of iron in Fe_3C .

of major fraction of particles, and both the ZFC and FC curves coincide at high temperatures—the temperature of deviation (T_B of the largest particles) is labelled as T_{DIFF} . The discrepancy between T_{MAX} and T_{DIFF} , that should be equal in the ideal case of a SPM system, signals the particle size distribution in the sample.

In case of commercial SWCNTs, the blocking temperatures T_{MAX} are 35 K at 10 mT in case of the HiPco_raw and 26 K at 10 mT for HiPco_SP, samples, respectively and T_{DIFF} are 202 K for the HiPco_raw and 278 K for HiPco_SP samples, respectively. Also the reduction of the T_{MAX} in increasing magnetic field, typical for such a system, has been observed (inset in Figure 3). Shift of the T_{MAX} to the lower temperature in case of the HiPco_SP sample could be attributed to the reduction of particle size or inter-particle interactions.

Inspecting the low temperature part of the FC curve of the HiPco_raw SWCNTs, the small saturation of the magnetization was observed, signaling the presence of weak inter-particle interactions. Saturation of the FC curve of the HiPco_SP sample is negligible, which is not surprising because the amount of magnetic metal is at least six times lower than in case of the HiPco_raw sample, suggesting better dilution of particles within the sample leading to the minimization of inter-particle interactions. In an ideal case of a SPM system without interaction, the FC curve should obey the Curie-Weiss law. Thus plotting the temperature dependence of inverse magnetization (result for the HiPco_SP sample is illustrated in the inset of Figure 3), resulting curve

should be linear. The non-linearity of such curve was observed for both samples, as a consequence either of inter-particle interactions (more significant for the HiPco_raw sample), particle size distribution (the HiPco_SP sample) or combination of both of these effects.

The measurement of magnetization isotherms provided the additional information about structure of magnetic nanoparticles in both samples. The hysteresis (typical feature of the block state below the T_B) was observed at 2 K with the symmetric values of coercivity, H_C for opposite polarities of magnetic field, reaching values of 150 mT for the HiPco_raw and 102 mT for the HiPco_SP samples, respectively (Figure 3). The decrease of the coercivity points at the reduction of the nanoparticle size or inter-particle interactions in the HiPco_SP sample. The magnetization isotherms above the T_B were analyzed by using the fit of generalized Langevin function and the average magnetic moments per particle has been calculated. Knowing both the magnetic moment of the particle and that of the unit cell (μ_c equal to $21.6\mu_B$ [Shein *et al.*, 2007]), it is possible to calculate the volume and subsequently the “magnetic” size of the particle (Table 1). It is obvious that the “magnetic size” of the particle in the HiPco_raw sample is larger than the size of the particle calculated from the diffraction pattern. The discrepancy could be explained by the so-called core-shell model of the particle with the well crystalline and magnetically ordered core (which contributes to the diffraction) and an amorphous shell, which only increases magnetic moment of the particle by a linear, paramagnetic-like term. Increase of magnetic size of the nanoparticles of the HiPco_SP sample in comparison with the HiPco_raw sample could be either the result of the real increase of particle size in the HiPco_SP sample or more probably it means that the shell part of the particles in the HiPco_raw sample which decreases the resulting magnetic moment has been removed and this explanation is valid whether the part of the shell of the HiPco_raw nanoparticles is not only amorphous, but also paramagnetic. This assumption is confirmed also by reduction of linear paramagnetic contribution to the HiPco_SP magnetization isotherm measured at 300 K with respect to the HiPco_raw sample.

Regarding discussion on magnetic properties of commercial SWCNTs, following idea can be deduced from the results obtained on purified SWCNTs. In case of the HiPco_400 sample, the annealing in air lead to the sintering of particles (as could be deduced from the saturation of the low temperature part of the FC curve and shift of T_{MAX} to the much higher values, with the diameters of particles ranging for 4.2 to 6 nm). Mild acid treatment probably leads to the removal of the most of the particles (little saturation at the beginning of the FC curve is the consequence of dilution of particles in the sample, thus of their partial removal).

Annealing of SWCNTs at 1200 °C (the HiPco_1200 sample) lead to (1) reduction of number of particles (proved by only little saturation of the FC curve), (2) highly probably lead to partial removal of paramagnetic shell (as it could be deduced from almost similar course of magnetization isotherms measured at 2 and 300 K, Figure 6), and (3) further sintering of remaining particles, as could be viewed from increase of

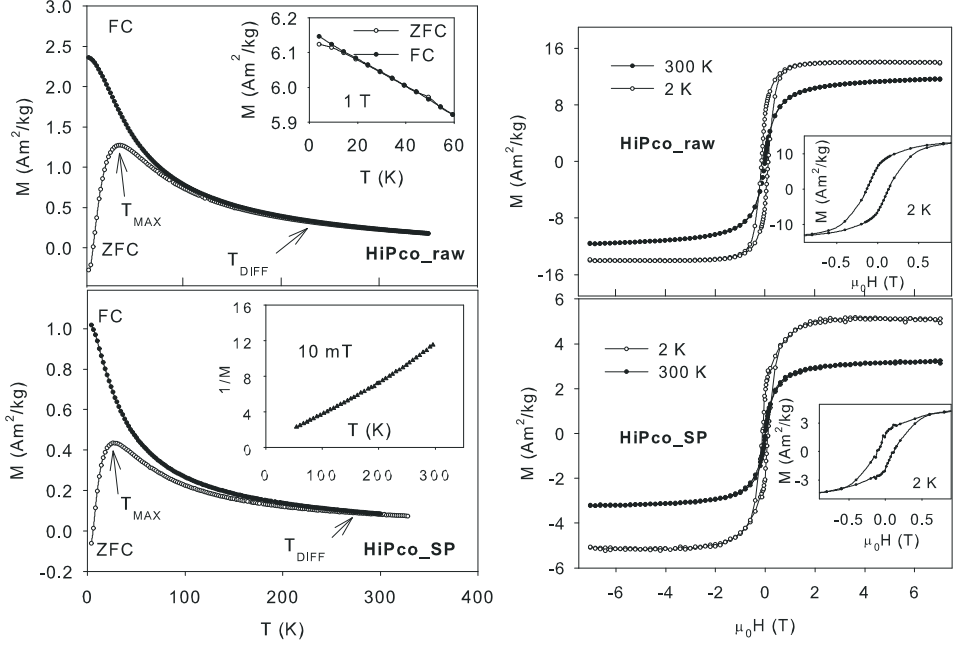


FIGURE 3. Left: The temperature dependence of the ZFC and FC magnetization measured at 10 mT for the HiPco_raw and HiPco_SP samples. The curves measured at 10 mT and 1 T and the inverse dependence of magnetization are in the insets. Right: Magnetization isotherms measured at different temperatures for the HiPco_raw and HiPco_SP samples, respectively. The detail of the loops measured at 2 K are in the inset.

TABLE 1. Median, μ_0 and mean, μ_m magnetic moment connected by relation $\mu_0 = \mu_m \exp\left(-\frac{\sigma}{2}\right)$, with the appropriate magnetic diameters, d_0 and d_m , compared with particle diameters calculated from blocking temperatures, d_{TDIFF} and d_{TMAX} .

Sample	$\mu_0 \times 10^3$ (μ_B)	d_0 (nm)	σ	$\mu_m \times 10^3$ (μ_B)	d_m (nm)	d_{TMAX} (nm)	d_{TDIFF} (nm)
HiPco_raw	1.3 (2)	2.6 ± 0.8	0.59	0.9 (2)	2.4 ± 0.3	2.4 ± 0.4	4.3 ± 0.5
HiPco_SP	2.0 (2)	3.0 ± 0.7	0.58	1.5 (2)	2.7 ± 0.3	2.2 ± 0.5	4.7 ± 0.7
HiPco_1200	4.8 (2)	4.0 ± 0.6	0.22	4.3 (2)	3.8 ± 0.3	3.7 ± 0.5	10.0 ± 0.9

magnetic size calculated from fitting the unhysteretic data by the Langevin function (Figure 6, Table 1).

Magnetic measurements performed on the HiPco_2200 sample showed that the magnetic response was purely diamagnetic (Figure 6). Together with the result from

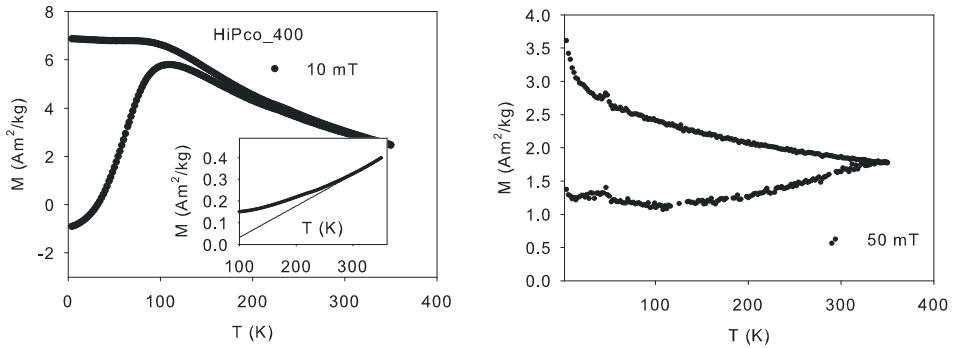


FIGURE 4. The temperature dependence of the ZFC and FC magnetization measured at 10 mT for the HiPco_400 sample after annealing step with the insert dependence of magnetization in the inset (left) and after the mild acid reflux (right).

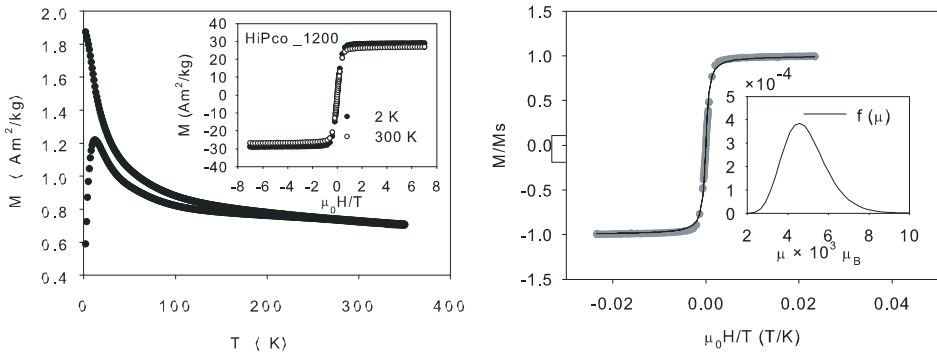


FIGURE 5. The temperature dependence of ZFC and FC magnetization measured at 10 mT for the HiPco_1200 sample with the magnetization isotherms in the inset (left). The example of the fit of the weight sum of the Langevin function to the data at 300 K in Langevin scaling the moment distribution function in the inset.

TG measurement, we should state that there is the undetectable amount of metal. As was claimed in the introduction, to study magnetism on SWCNTs, sample should contain no metal, thus further investigation of atomic traces of iron within the samples are required.

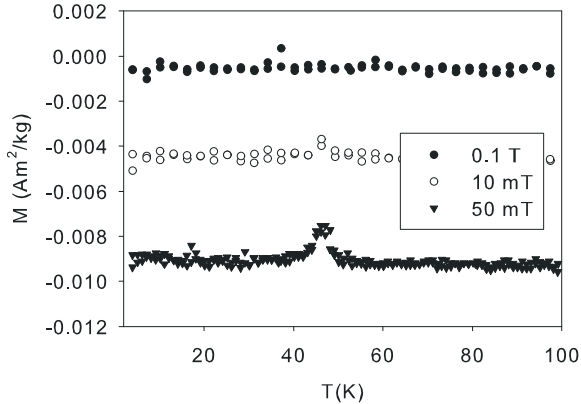


FIGURE 6. The temperature dependence of the ZFC and FC magnetization for the HiPco_2200 sample.

4. Conclusion

We have investigated structural and magnetic properties of the residual Fe catalyst in the commercial HiPco_raw and HiPco_SP (super-purified) SWCNTs, respectively. The S-XRD and Mössbauer spectroscopy confirmed presence of Fe in the HiPco_raw SWCNTs, most in the form of cementite, Fe_3C . Size of the nanoparticles in the HiPco_raw sample was determined from the S-XRD, leading to the mean diameter value equal to 1.9 nm. Results of magnetic measurements pointed at the core-shell structure of the particles, with the amorphous paramagnetic shell and the crystalline core. Even if the HiPco_SP sample should contain less than 5 wt% of metal, as it has been demonstrated, this metal is also in the form of weakly-interacting SPM nanoparticles with the blocking temperature at 26 K, pointing either at the decrease of particle size with respect to the HiPco_raw sample or reduction of inter-particle interactions. The increase of mean magnetic moment and “magnetic” diameter of particles together with the decrease of coercivity and reduction of linear paramagnetic part in magnetization isotherms measured at 300 K finally confirmed the decrease of particles size due to the removal of paramagnetic shell. Besides that, it has been demonstrated that the HiPco_SP SWCNTs are not suitable for reliable studies of CNTs magnetism because further removal of metal catalyst particles is required.

Inspecting magnetic properties of purified HiPco_raw SWCNTs resulted in possible sintering and removal of nanoparticles in low temperature annealed and mild acid treated HiPco_400 sample, partial reduction of paramagnetic shell and subsequent sintering of nanoparticles. Diamagnetic response of high temperature annealed HiPco_2200 sample together with the undetectability of metal via thermogravimetry suggested that this method lead to complete removal of metal particles and gave much

better purity than commercially treated SWCNTs (HiPco_SP). Further investigation of purity on atomic scale and structure of treated nanotubes are required.

References

- BITTOVA, B. ET AL.: *J. Phys. Chem. C* **115**, 17303 (2011).
ESQUINAZI, P. ET AL.: *Phys. Rev. Lett.* **91**, 227201 (2003).
DRESSELHAUS, S., DRESSELHAUS, G., AVOURIS, PH.: Carbon nanotubes: synthesis, properties, structure and applications. Springer-Verlag, New York 2001.
KNOBEL, M. ET AL.: *J. Nanosci. Nanotechnol.* **8**, 2836 (2008).
MAKAROVA, T. ET AL.: *Nature* **413**, 22 (2001).
MONTHIOUX, M. ET AL.: *Carbon* **39**, 1251–1272 (2001).
MORADIAN, R., FATHALIAN, A.: *Nanotechnology* **8**, 17 (2006).
NEEL, L.: *Ann. Geophys. (C.N.R.S.)* **5**, 99 (1949).
ORELLEANA, W., FUENTHEALBA, P.: *Surf. Sci.* **600**, 22 (2006).
RON, M., MATHALONE, Z.: *Phys. Rev. B* **4**, 774 (1971).
SHEIN, I. R., MEDVEDEVA, N. I., IVANOVSKII, A. L.: *Phys. Stat. Sol. B* **244**, 22 (2007).
VEJPRAVOVA, J. ET AL.: *J. Appl. Phys.* **97**, 124304 (2005).
WILES, D. B., YOUNG, R. A.: *J. Appl. Cryst.* **15**, 430 (1982).